Systematic experiments to quantitatively assess image quality for CT scans of a Karoo tetrapod fossil

Muofhe Tshibalanganda[1] §, Anton du Plessis[1,2]*, Stephan G. Le Roux[1], Wendy L. Taylor[3], Roger M.H. Smith[4,5] & Claire Browning[4]

[1]*CT Scanner Facility, Stellenbosch University, Stellenbosch, South Africa*

[2]*Physics Department, Stellenbosch University, Stellenbosch, South Africa*

[3]*University of Cape Town, Cape Town, South Africa*

[4]*Iziko Museums of South Africa, Cape Town, South Africa*

[5]*Evolutionary Studies Institute, University of the Witwatersrand, Johannesburg, South Africa*

Received 10 April 2018. Accepted 3 May 2019

Over the past decade non-destructive, three-dimensional visualization and analysis of fossils using X-ray tomography has greatly advanced palaeontological studies worldwide. Micro-computed tomography (microCT) is now accepted as best practice in palaeontological studies to augment the anatomical description of newly discovered fossils. Despite advances in laboratory microCT hardware, software and skills of users, there is a lack of clear methodologies for scanning and analysing fossils. Here we report on a systematic and detailed study of the quantitative effects of the variation of different microCT scanning parameters on the image quality of an unprepared fossilized Karoo tetrapod skull and parts of the postcrania. Results indicate that voltage variations do not increase the contrast for the bone as one would expect, and the best image quality solution is found using high frame averaging and high X-ray flux (current). Although this study was limited to one specimen, the results may find a practical use for future studies involving similar fossils.

Keywords: MicroCT, image quality, X-ray tomography, palaeontology, Karoo, fossil.

INTRODUCTION

Micro X-ray computed tomography (microCT) is known in palaeontology as a method for providing 3-D virtual visualization and analysis of fossils, some of which are still encased in solid rock. MicroCT has enabled the non-destructive visualization of internal structures of a variety of fossils (Lukeneder *et al*. 2014). This 'virtual palaeontology' has allowed palaeontologists to gain new insights into fossil morphology, anatomy, development and their preservation (Abel *et al*. 2012; Klages 2013; Cunningham *et al*. 2014; Dawson *et al*. 2014; Fisher *et al*. 2014; Rahman & Smith 2014; Liu *et al*. 2015; Reid *et al*. 2018) and it has become standard practice to use microCT in paleontological descriptions. The relatively recent application of microCT to Karoo tetrapod fossils has enabled palaeontologists to gain insights into topics such as fossil tooth replacement in cynodonts (Jasinoski *et al*. 2015), the architecture of osseous capsules in dicynodonts (Araújo *et al*. 2018), volumes and shapes of braincases in dinosaur skulls (Chapelle *et al*. 2018) and the functional evolution of anatomical traits (Benoit *et al*. 2016, 2017; Lyson *et al*. 2016; Sobral *et al*. 2016). These researchers typically relied on varying microCT parameters to overcome the challenges described above (Abel *et al*. 2012; Rahman *et al*. 2012; Smilg 2017). High quality microCT data is not only important for visualization but also for the ability to extract adequate quantitative information for the required research question (Du Plessis *et al*. 2016).

Despite this growing interest in virtual palaeontology, microCT is still perceived as a financial risk as there is no detailed methodology available for scanning fossils, and therefore scans are not always successful. Some of the challenges include: (1) the fossil and enclosing matrix having similar X-ray densities which leads to difficulty in virtually extracting fossils inside rock; (2) penetration difficulties for X-rays due to dense rock minerals resulting in not being able to visualize fine details of the preserved fossil or even failed scans; and (3) dense particles and inclusions causing image artefacts which mask features and make 3D visualization impossible (Cunningham *et al*. 2014; Rahman & Smith 2014; Sutton *et al*. 2014).

MicroCT scanning of Palaeozoic and Mesozoic tetrapod fossils from the Karoo Basin of South Africa shows that they are susceptible to all of the challenges above. Permian- to Jurassic-aged continental strata make up the 8000 m thick Karoo Supergroup, covering two-thirds of the surface area of South Africa. These rocks are world-renowned for their abundant and diverse vertebrate fossils, in particular, the 100-million-year-long evolutionary record of therapsids (mammal-like reptiles) leading to the origin of mammals. Karoo vertebrate fossils are

*Author for correspondence. E-mail: anton2@sun.ac.za

***Palaeontologia africana* 54: 1–13 — ISSN 2410-4418 [Palaeontol. afr.] Online only**
Permanently archived on the 20th of August 2019 at the University of the Witwatersrand, Johannesburg, South Africa
The article is permanently archived at: http://wiredspace.wits.ac.za/handle/10539/27891

preserved in rocks dating back 300 Ma through to 190 Ma (Smith *et al*. 2011). Consequent to their initial deposition, the depth of burial and degree of diagenesis have had a fundamental influence on their mode of preservation. They are mainly preserved in non-marine sandstones and shales deposited in a wide range of environments from glacial meltwater lakes to temperate floodplains and hot desert dunes. After burial, early diagenetic calcification (and in some cases ferruginization) of the bone cavities and interstitial spaces in the surrounding matrix commonly formed a hardened nodule around the bone (Smith 2000). With deeper burial, metamorphic fluids led to silicification and, in many cases, the iron was remobilized into haematite crusts and crystals. These dense haematite inclusions cause image artefacts in microCT images. The similarity of density between fossil bone and the enclosing rock makes some parts of the fossil bone almost identical in X-ray density to the surrounding rock, while other parts, such as teeth, are more X-ray dense, due to higher levels of calcium, phosphate and other minerals present. These variables and artefacts make Karoo tetrapod fossils a challenging case study for producing high quality microCT images. The density of iron and related metals cause excessive X-ray absorption compared to the materials surrounding it, causing streaky (star-shaped) artefacts in CT images. This is mainly due to some X-ray images being entirely masked by the inclusions in the line of sight behind the mineral inclusion, causing errors in reconstruction.

The image quality of a scan is influenced by several factors (Cantatore & Müller 2011) including X-ray parameter settings, reconstruction settings, and image processing (filtering). This case study demonstrates a systematic series of scans of the same sample containing fossil bone. The parameters are varied based on parameter variations described previously for biological samples (Du Plessis *et al*. 2017), but their relative importance is quantitatively demonstrated here for a typical fossil scan. In addition to scan parameters, the reconstruction, post-processing and ease of segmentation are discussed. Finally, we present a table summarizing the key findings. These findings might be useful for Karoo palaeontologists as a starting point for obtaining high quality microCT scans of similar rock-embedded fossils. We expect them to apply to all fossils embedded in similar relatively homogenous well-cemented sedimentary rock (i.e. sandstone, siltstone, mudstone and limestone) and highlight some important parameters for successful use of laboratory microCT for virtual palaeontology in general.

MicroCT, which is also known as industrial X-ray computed tomography, is a specialized form of computed tomography for non-medical application. A typical microCT setup (Fig. 1) consists of an X-ray source, rotation table, and X-ray detector. X-rays are generated in a cone beam by an X-ray tube and are directed through and around a rotating sample. The detector converts attenuated radiation through the sample into 2D projection images (Fig. 1). The 2D projection images are then used to

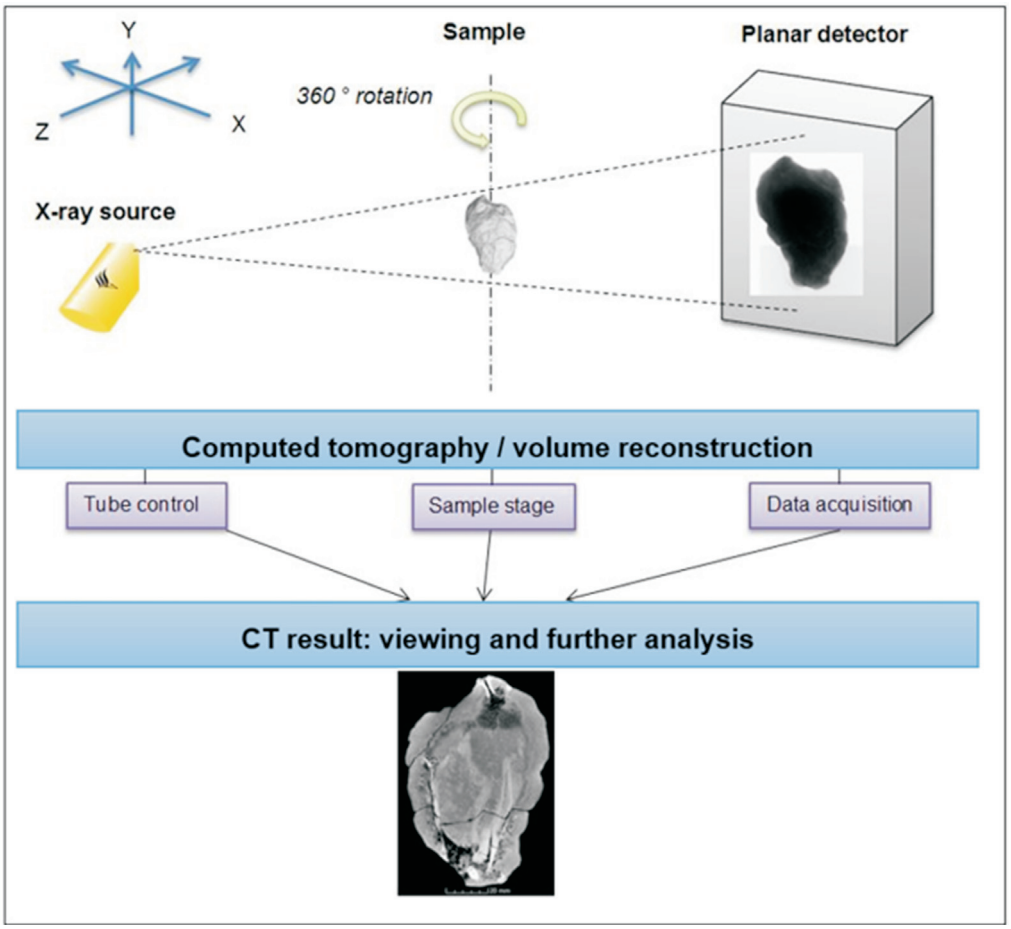

Figure 1. Schematic diagram of microCT scanning, reconstruction and visualization.

reconstruct a 3D data set that can be viewed and analysed by a variety of software packages (Cantatore & Müller 2011; Du Plessis *et al*. 2017). After reconstruction, all image processing and analysis discussed in this work takes place in the last step (Fig. 1) – on a computing workstation.

MATERIALS AND METHODS

A 245 million year old Mid-Triassic tetrapod fossil (SAM-PK-K10180) from the Karoo Supergroup (Fig. 2) housed in the department of Karoo Palaeontology, Iziko South African Museum in Cape Town was scanned using a Phoenix V|Tome|X L240 (General Electric Sensing and Inspection Technologies Phoenix X-ray, Wunstorff, Germany) microCT system located at the CT Scanner Facility of the Central Analytical Facility (CAF), Stellenbosch University, South Africa (Du Plessis *et al*. 2016). The fossil, now been identified as the skull and parts of the postcrania of a basal rhyncosaur, is completely encased in a carbonate-rich, micritic mudstone nodule some 10 cm in diameter and 6 cm thick and it had not been manually prepared before scanning. All reconstructions were conducted using system-supplied DATOS 2.0 software (General Electric Sensing & Technologies). Images were obtained and analysis performed using the VGSTUDIO MAX 3.1 software (Volume Graphics GmbH, Heidelberg, Germany).

A series of scans were performed individually to test the effects of; (1) varying voltage, (2) current, (3) beam filtering, (4) reconstruction options (beam hardening correction and reconstruction filtering) and (5) post-process filtering on image quality. Initial efforts at defining image quality metrics were complicated by the fact that the fossil bone and rock are not homogenous, and therefore the best indicators of image quality for fossil scans used in this work were: fossil bone/rock grey value, fossil bone/rock edge sharpness, and background noise. The fossil bone/rock grey value in this work was calculated as the ratio of mean grey values of small cubic regions of interest representative of bone and of the rock, using the same regions for each series of scans (Fig. 3). Edge sharpness was measured as the gradient of the slope between two materials, using the minimum and maximum values of the two materials; a 10–90% slope gradient is measured (Fig. 3b). Obtaining the best edge sharpness is important to palaeontological applications as it allows for an accurate and less time-consuming segmentation of a fossil inside a rock. The image background noise was measured from the same size (X = 1.48, Y = 1.40 and Z = 0.8) uniform region of interest (ROI) taken on the background air as shown by the blue block in (Fig. 3a). The noise value was measured as the standard deviation of the mean grey values taken from the volume of the ROI.

X-ray tube voltage determines the penetration ability of the X-rays (highest keV value of the polychromatic beam increases with increasing tube voltage), while current affects the amount of radiation (photon flux or intensity of the beam) without modifying the penetration ability of

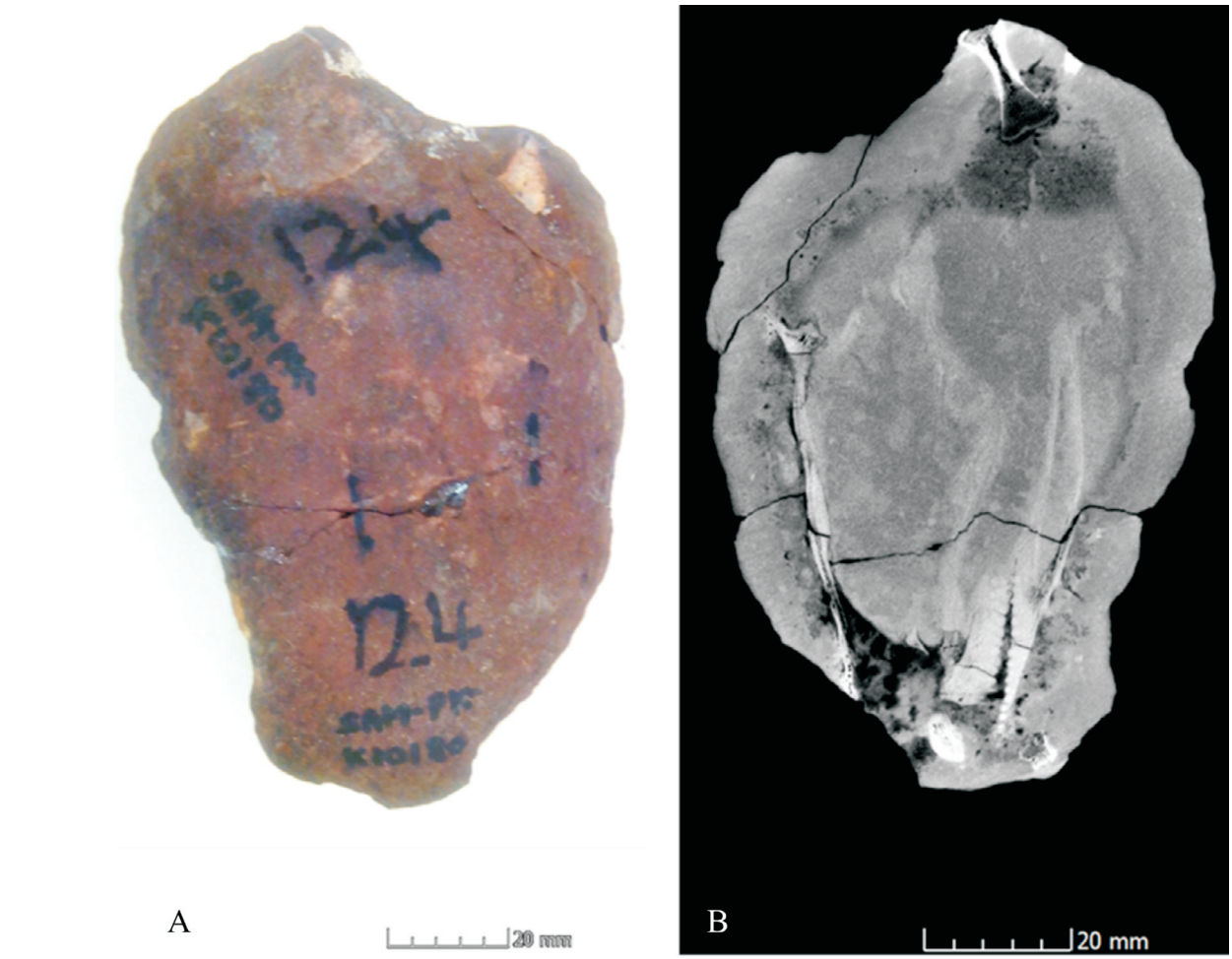

Figure 2. Karoo fossil encased in sedimentary rock, SAM PK K10180 (6.6 × 2.4 × 10.7 cm) (**A**) and CT slice image of the sample (**B**).

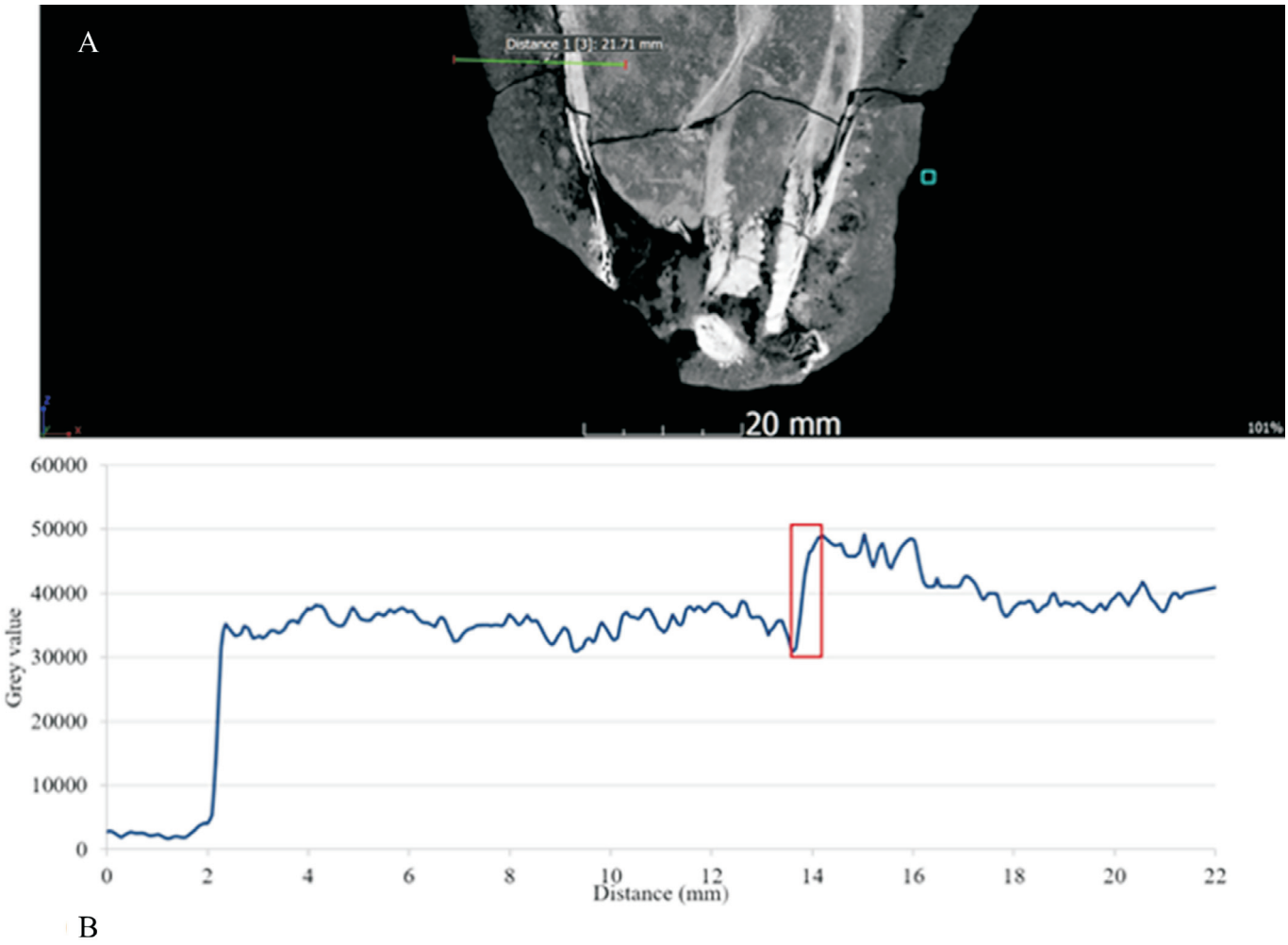

Figure 3. 2D slice image of SAM PK K10180 showing the region of interest for background noise measurement (blue block) (**A**) and the line profile taken across the fossil bone – rock interface for edge sharpness measurement. The red box on the line profile indicates where the edge sharpness was calculated and the green line in the CT image shows where the line profile was taken (**B**).

the emission spectrum (Cantatore & Müller 2011). To aid the interpretation of results from this experiment, no beam filters were added while changing the voltage. However, to maintain constant signal levels on the background (intensity on the detector), higher voltage scans (which generally have higher intensity on the detector) were conducted with lower current values, in order to reduce the total intensity of the beam without changing any other parameters. It was expected that beam filters, acquisition timing or detector sensitivity/amplification settings might change the noise levels and complicate the results obtained. The effect of current increase is an increased beam intensity, while voltage changes the beam's emission spectrum. Therefore small changes in current to allow the same intensity on detector may be attributed to voltage alone. Nevertheless, an additional experiment was conducted. This additional experiment was conducted with a chicken bone and three sandstones attached to the chicken bone by tape to simulate a bone embedded in rock. The chicken bone and rocks used have significantly varying composition – more so than would be expected of fossil bones compared to host rock. In this experiment, three scans were conducted at varying voltages. In this case, the current was kept constant and the detector sensitivity was adjusted to maintain the same intensity on the detector. The effect of voltage variation was therefore investigated using two variations of experiments, by adjusting either the current or detector sensitivity.

For the subsequent experiment testing the variation of current alone, the higher-current scan, which causes higher intensity at the detector, was done with shorter acquisition time to allow a similar background signal level.

The effect of beam filtering was analysed separately. Beam filtering is often applied to compensate for beam hardening that might occur (Ketcham & Carlson 2001; Du Plessis *et al*. 2017). This is achieved by placing a filter between the X-ray source and the sample. At 180 kV and varying the current to maintain constant background count (intensity), copper filters varying in thickness from 0.1 mm to 1 mm were used, to investigate beam hardening directly. Beam hardening occurs when low energy photons of the X-ray beam are absorbed in a sample more than the high energy X-rays, resulting in a cupping artefact around the sample edges (Cantatore & Müller 2011; Du Plessis *et al*. 2017).

Image averaging or frame averaging is typically used to reduce noise by averaging images during scanning. Increasing image averaging was applied on scans with settings of 180 kV and 70 μA.

In addition to scan parameters described above, various options for reconstruction and post-processing (readily available in commercial software packages) were investigated. The aim was to check the relative importance of each of the image-processing steps. Reconstruction software involves a series of choices, which might affect the image quality of the obtained reconstructed 3D data (Cnudde & Boone 2013; Du Plessis *et al*. 2017). Reconstruction options evaluated in this study are beam hardening correction and reconstruction filtering, both of which are easily implemented in commercial reconstruction software packages. Beam hardening correction addresses the cupping artefacts that might occur at sample edges. The cupping effect causes the appearance of bright sample edges compared to the rest of the sample as a result of beam hardening.

Filtering is a noise reduction image processing technique used for modifying or enhancing an image during reconstruction or during post-processing. Reconstruction filtering involves image filtering during reconstruction in the Datos software package – specific options considered were inline median, volume filters and edge enhancement. After reconstruction, the post-processing filters applied in VGSTUDIO MAX was median, adaptive gauss, and the non-local means filters.

RESULTS AND DISCUSSION

Image quality changes in all scans were quantified as a function of varying parameters, in order to find optimal scan settings for Karoo fossils inside the rock, and to highlight the relative importance of various parameters. This involves a comprehensive series of experiments comprising of 18 full scan data sets. Each parameter investigated is described separately below.

Voltage

Voltage is a scan parameter that determines the penetration ability of the X-ray beam and needs to be high enough to allow good visualization of internal features. Typically, denser and larger samples require higher voltage to allow enough X-ray penetration to get appropriate contrast between materials. When the voltage is not high enough, the interior of the sample becomes noisy, and features cannot be distinguished. For smaller and lower density samples, typically lower voltages allow better contrast especially between different materials – due to differences in material X-ray absorption coefficients. In this case study, varying the voltage showed no changes in scan quality as shown by the 2D slice images and bar charts (Fig. 4). The noise and the edge sharpness also did not show any significant change with varying voltage (Fig. 5).

These results may be explained by a competition between two major influences on the obtained contrast between the materials. Firstly, lower voltage improves contrast according to X-ray attenuation coefficient differences between materials. Secondly, lower voltage results in poorer penetration of the sample resulting in less contrast between materials. With these two competing effects, the result is that voltage changes do not affect the contrast for this particular type of sample. To resolve if this is a general result for all similar samples, an additional experiment was devised. As an extreme case of compositional difference which should be easy to detect by microCT, a chicken bone with attached rocks were used and scans conducted at three different voltages. The result was similar as above, with very little change seen in the contrast between bone and rock (see Fig. 6). In this case, the higher voltage seemed to increase the contrast between bone and rock slightly. The conclusion remains the same: varying voltage does not make as large a difference as expected. We speculate this is due to the need for good penetration of the samples, being dominant over any material-specific differences in X-ray absorption. This is for typical laboratory microCT systems and typical rock samples containing fossil bones, but might not be valid for the highly monochromatic and high-flux beams of synchrotrons. In that case, is it expected that lower voltages will be advantageous for material discrimination.

Current

Increasing the X-ray flux by increasing the current improved the scan quality significantly: the contrast between fossil bone and rock improved and finer details of the fossil anatomy could be visualized more clearly (Fig. 7). The edge sharpness between the fossil bone and the surrounding rock also increased with increasing current (Fig. 8), and the background noise remained constant. This result further supports the concept that the voltage is not the most important factor for this sample type but rather getting higher penetration – i.e. getting more X-rays through the sample – which can be done effectively by increasing current. It is important to note that as the current increases, the focal spot size increases and hence the effective resolution gets poorer – this is something that must be limited by the user. High current can also cause high local temperature in the X-ray tube target material causing costly damage and failed scans. A compromise between high current and voltage is therefore suggested. However, this result very clearly shows the significant improvement in image quality obtained by increased current.

Beam filtering

Beam filtering is often applied to pre-compensate for beam hardening that might occur. The results, as shown by the 2D slice images and the edge sharpness (Fig. 9), illustrate a general trend of improvement in image sharpness with increasing thickness of beam filters. However, there seems to be an optimal beam filter thickness for minimal noise at 0.2 mm in this case (Fig. 10). Increasing the filter thickness further is expected to reduce the X-ray intensity such that the image quality degrades as in lower current scans outlined above.

If beam hardening occurs, beam hardening correction in the reconstruction process can be used to reduce much of the cupping effect on the sample edges. An example of this is shown (Fig. 11), where the left scan shows the cupping effect on the sample edges and the right shows the beam hardening corrected scan. Apart from correcting the cupping effect, increased beam hardening correction

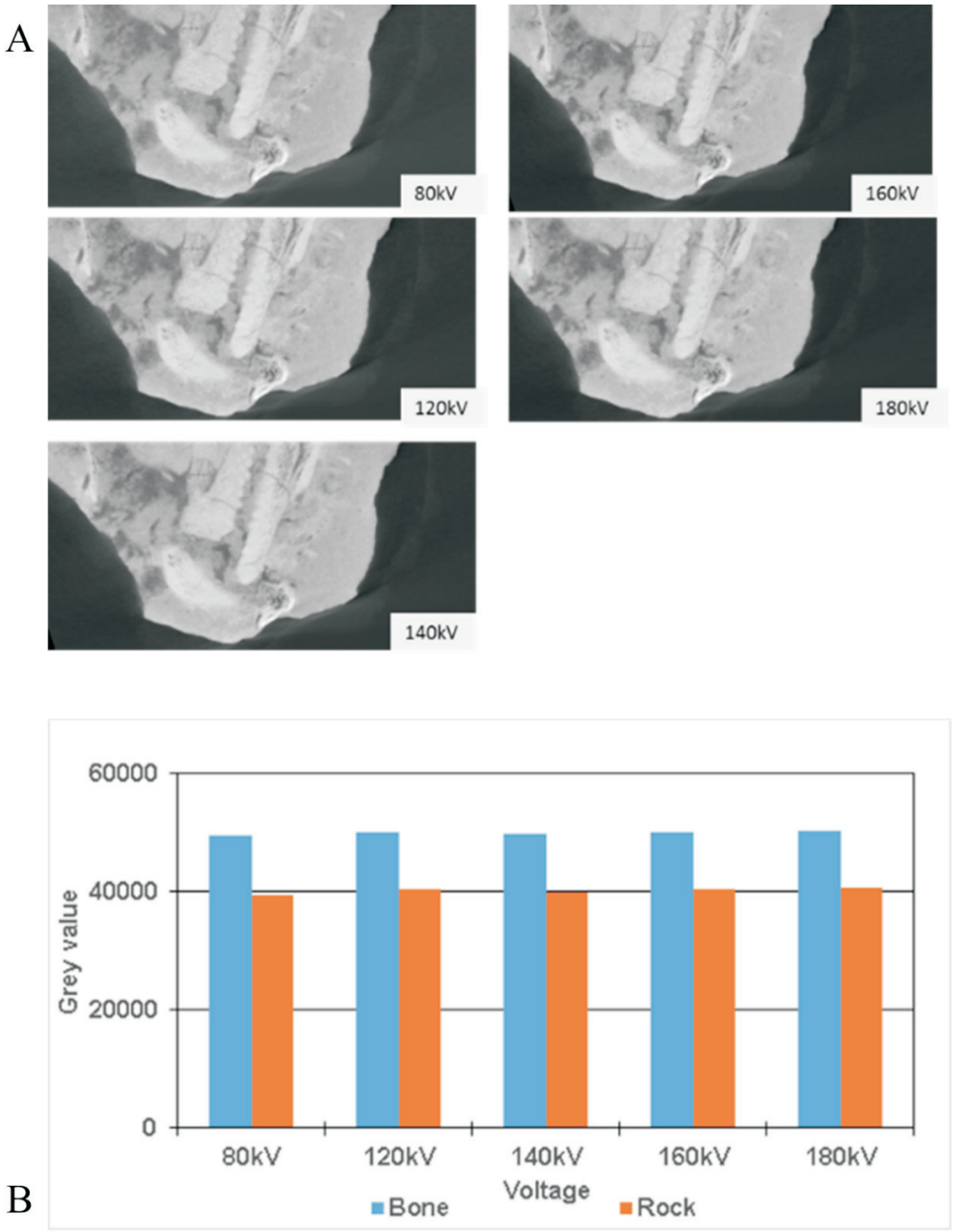

Figure 4. Effect of voltage change on scan quality evaluated by (**A**) visual impression in CT slice images and (**B**) grey values of representative regions of fossil bone and rock.

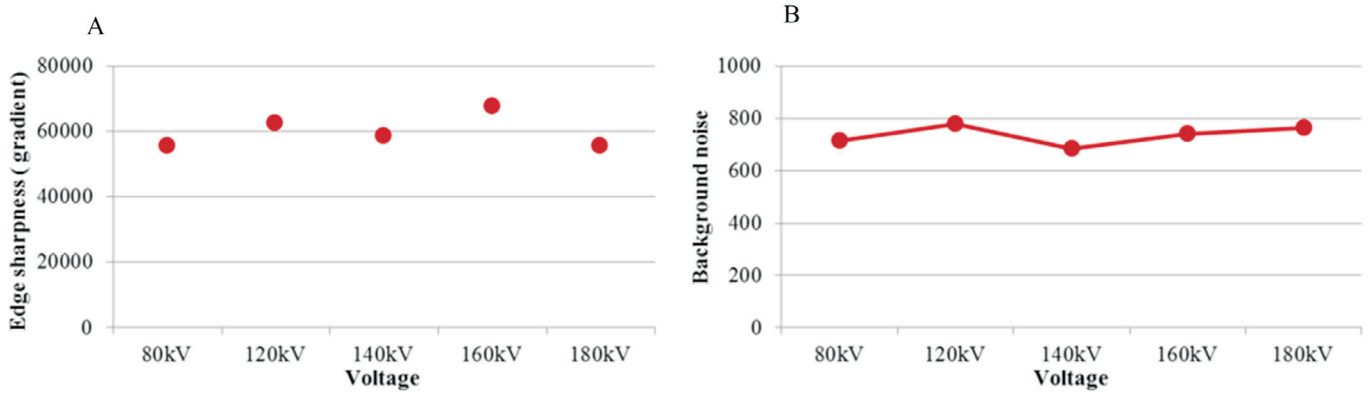

Figure 5. The effect of varying voltage on the image edge sharpness measured as the gradient of the slope between two materials (**A**) and background noise measured as the standard deviation of the mean grey values taken from the volume of the ROI (**B**).

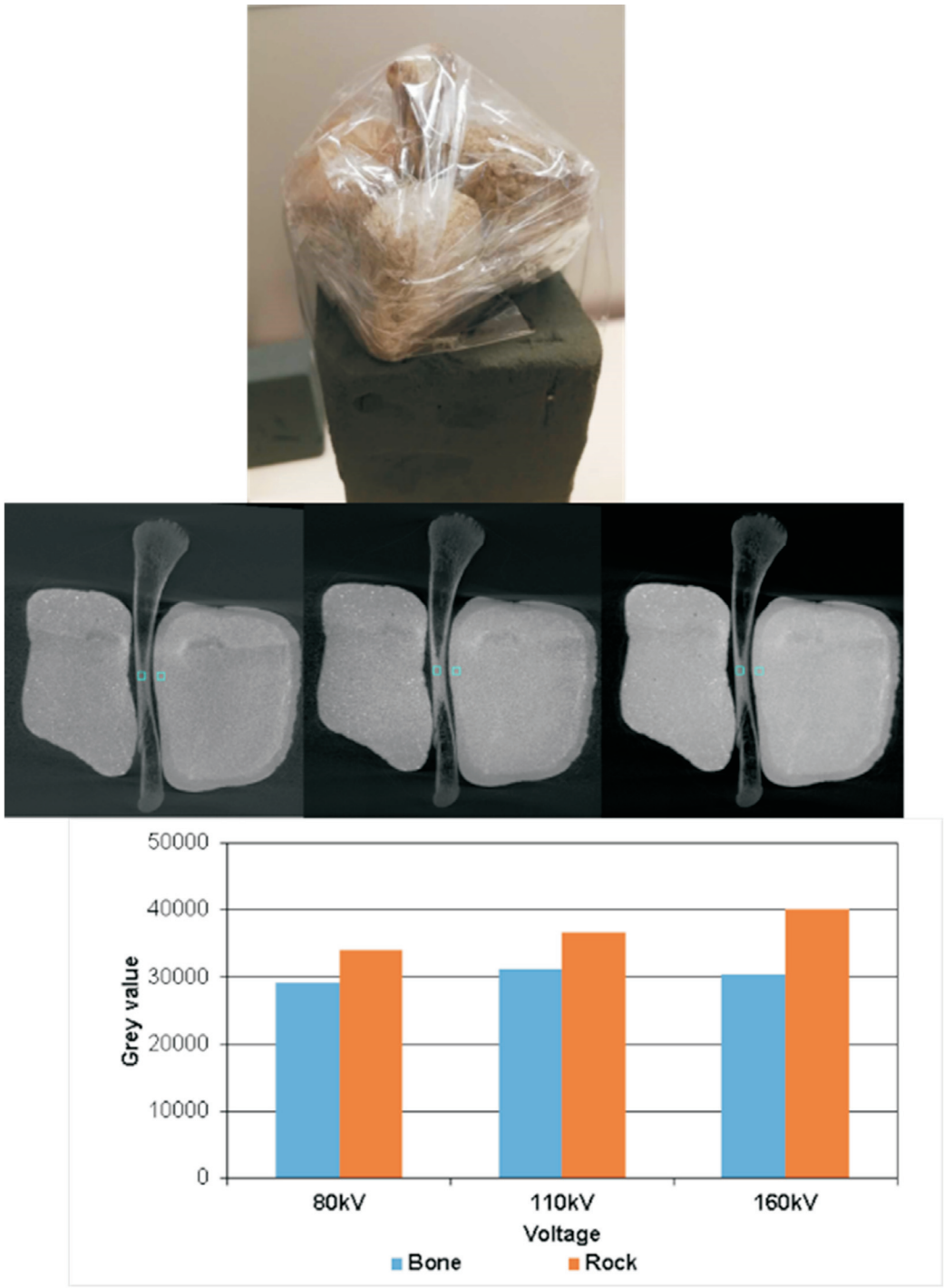

Figure 6. Simulated bone in rock with chicken bone and rocks taped to it – varying voltage and keeping current constant. The results show very little difference in material contrast.

increases the edge sharpness (see Fig. 12) allowing for more accurate and less time-consuming segmentation but this also increases the level of noise, so should be used with care.

Averaging

Increasing image averaging, where two or more images can be averaged at each rotation step during scanning, reduced the noise level and showed a slight increase in edge sharpness between the fossil bone and the surrounding rock (see Figs 13 & 14). However, increasing image averaging increases the total scan time which can be prohibitively costly to the user.

Reconstruction and post-processing filtering

The uses of reconstruction filtering and post-processing filtering were investigated quantitatively. The results showed that applying any filter reduces the level of noise as expected (see Fig. 15). Overall, the post-processing filter that showed the highest noise reduction was the relatively new (in commercial software) non-local means filter. There was no significant effect on the measured edge sharpness in any of the filter methods – for these typical settings (Fig. 15).

Excessive filtering can result in image blurring (see Fig. 16) where (A) is the unfiltered scan, (B) is the typical adaptive gauss filter and (C) is the adaptive gauss filter

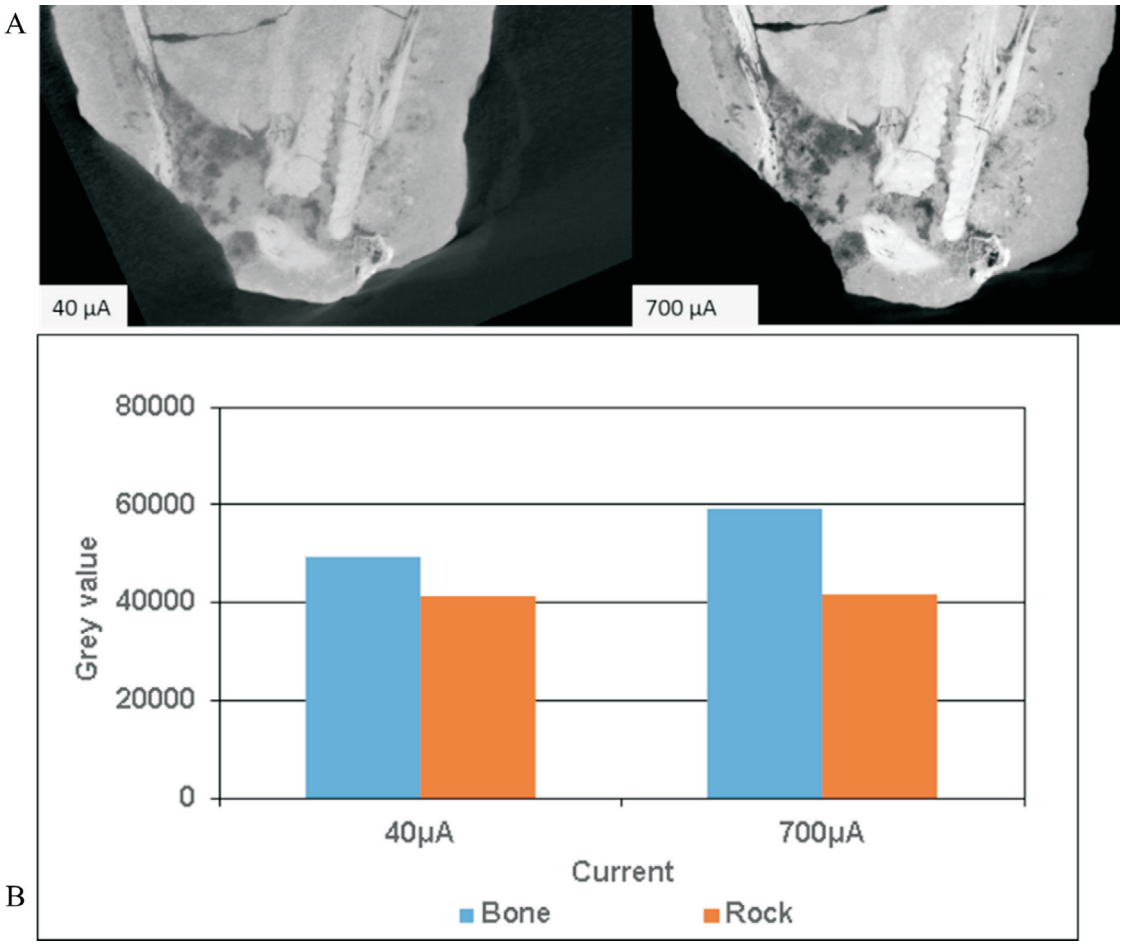

Figure 7. Increased current shows improved quality as evaluated by (**A**) 2D slice images and (**B**) grey values of representative regions of fossil bone and rock.

applied three times. Although the noise has decreased, the edge sharpness (Fig. 16) has also decreased making the distinction between the fossil and the rock difficult which consequently causes an unwanted loss in detail visibility. While the improvement in noise reduction is very useful (Fig. 15) excessive use of image filtering will cause loss of image sharpness (Fig. 16). Hence its use should be limited – especially when fine features are of interest.

High quality scan

As a demonstration of the above optimization for this type of sample, an optimized set of scan parameters was selected for comparison with a typical scan setup (which would usually be employed). In order to obtain high quality here, high current was used. In addition, for the selected voltage and current, image acquisition time and detector sensitivity was adjusted to allow high signal values on the detector. Table 1 shows the scan parameters employed to obtain the highest image quality for this Karoo fossil embedded in dense rock. The 2D slice images (Fig. 17) show a side-by-side comparison of the standard scan with the high quality scan.

A summary of the key findings in this work is provided in Table 2 for all parameters systematically investigated.

In summary, all parameters investigated (details of each scan) are presented in Table 3.

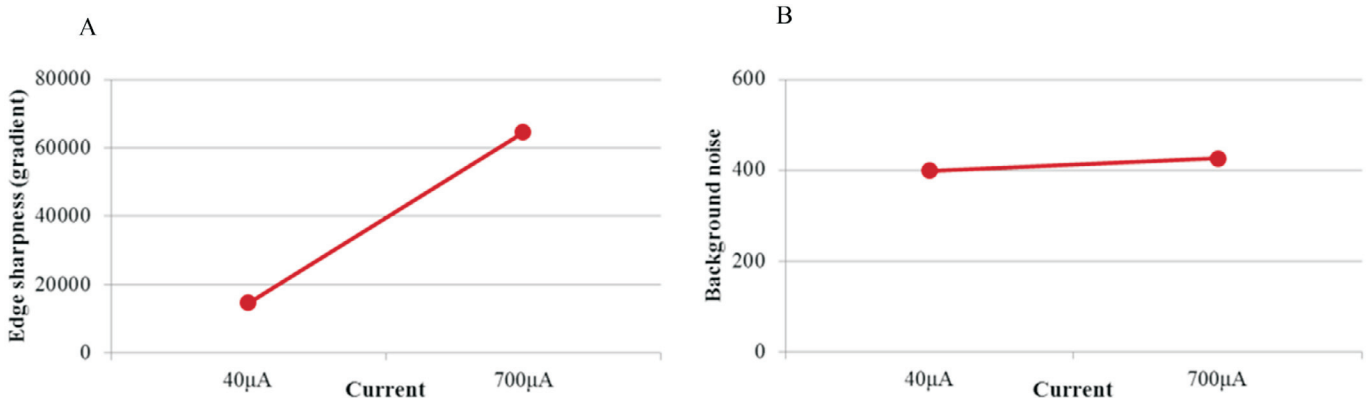

Figure 8. The effect of varying current on the image edge sharpness (**A**) and background noise (**B**).

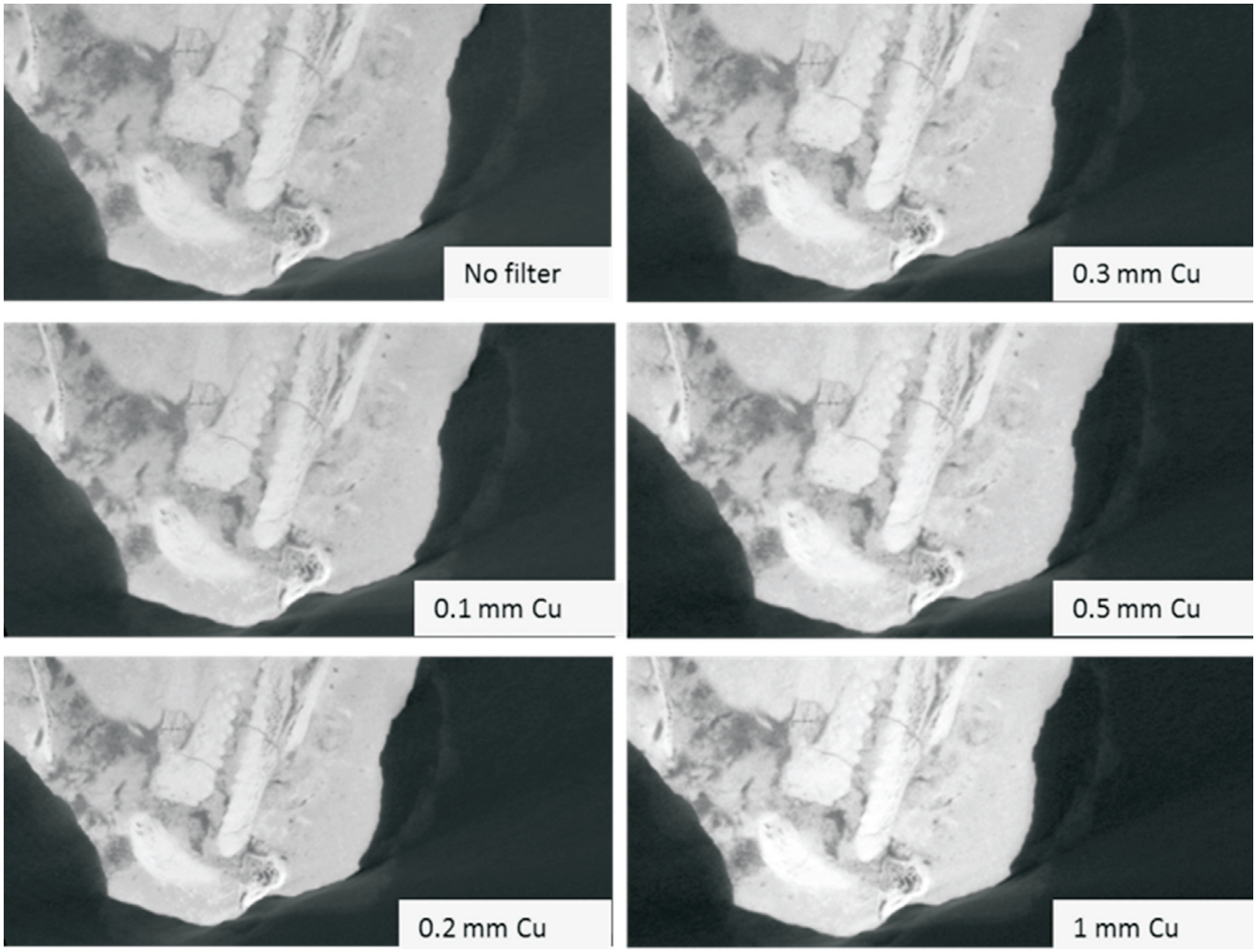

Figure 9. 2D slice images showing the quality change of varying scan parameter beam filtering.

CONCLUSION

It was found by systematic variation of parameters and quantitative measurement of image quality, that voltage does not play a major role in the contrast or image quality for this type and size of sample for laboratory microCT systems. Important parameters for increasing the quality of the scan data for this sample were found to be, in decreasing order of importance: (1) high current (high X-ray flux); (2) increasing signal values almost to saturation of the detector while keeping background noise low; (3) large amounts of image averaging during scanning – this refers to acquisition of more than one image at each rotational position and averaging these images which reduces the noise in the acquisition image and in the final reconstructed data, (4) strong beam hardening correction in reconstruction and (5) de-noising filters (post-acquisition) selectively applied to the final images. Clearly, there is a complex interrelationship for all parameters and the general rule is to first ensure artefact-free images, thereafter improve the contrast as far as possible. In order to

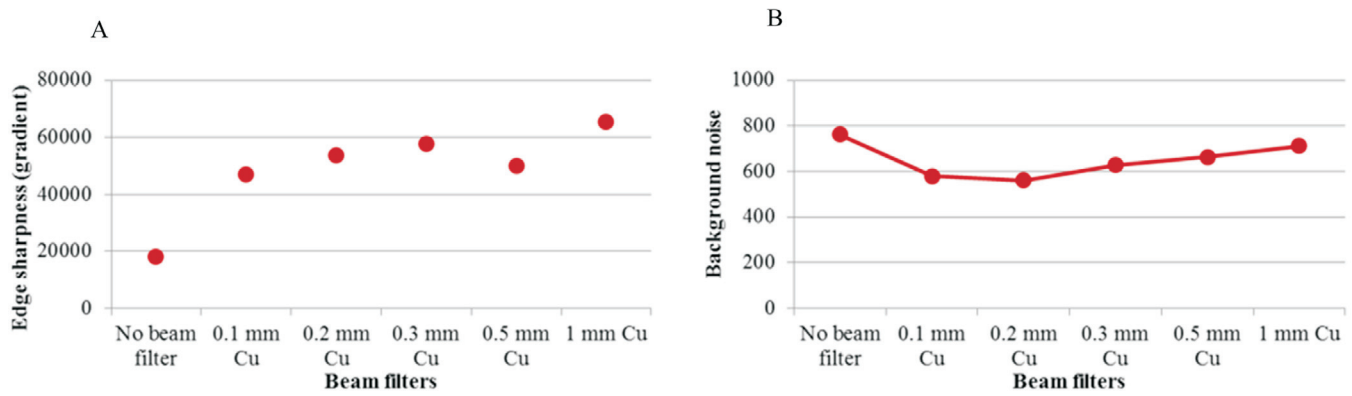

Figure 10. The effect of varying beam filters on the image edge sharpness measured as the gradient of the slope between two materials, using the minimum and maximum values of the two (**A**) and background noise measured as the standard deviation of the mean grey values taken from the volume of the ROI (**B**).

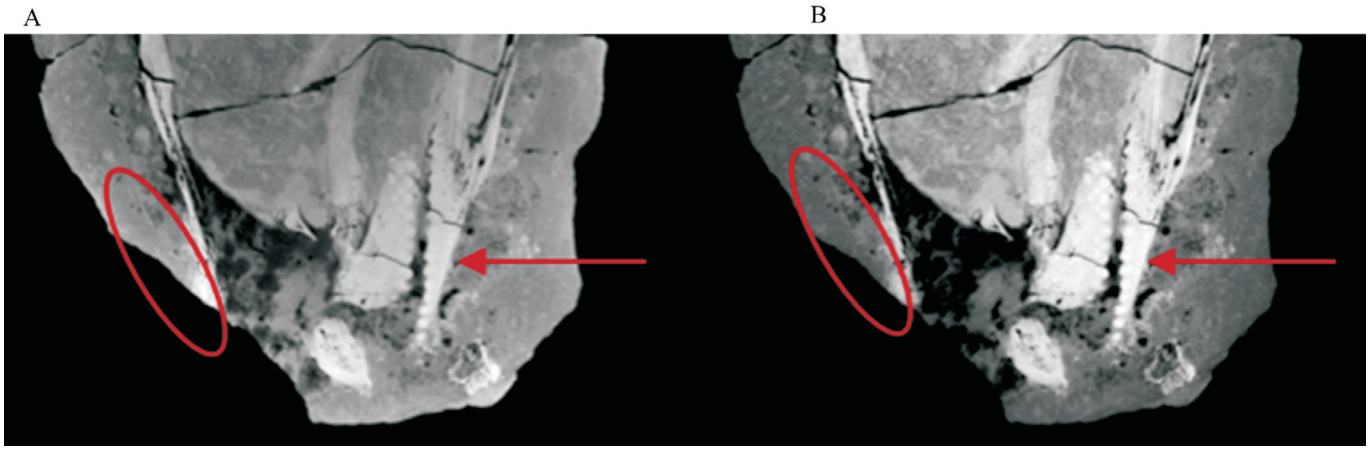

Figure 11. 2D slice images showing the results of beam hardening on a sample (**A**) *vs* a beam hardening corrected 2D slice image of the same data set (**B**).The cupping effect on the sample is shown by the red circle on the left slice image and the corrected cupping by the red circle on the right. The arrows point on the dark interior of the sample as result of beam hardening (**A**) and corrected beam hardening interior of the sample (**B**).

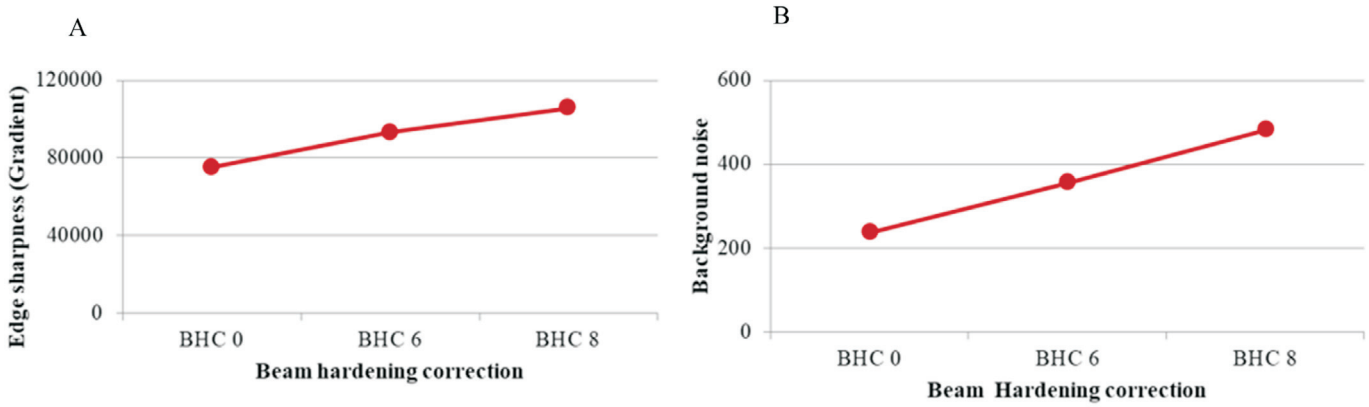

Figure 12. The effect of varying beam hardening correction on the image edge sharpness measured as the gradient of the slope between two materials, using the minimum and maximum values of the two (**A**) and background noise measured as the standard deviation of the mean grey values taken from the volume of the ROI (**B**).

ensure artefact-free images, a safe option is to use a relatively high voltage, to ensure no unwanted streak artefacts from inclusions that may be present. When the interest is in fine structures, parameter choice may prioritize improving edge sharpness – lots of acquisition image averaging and very little or no post-scan image filtering. In most cases, when the choice is based on strong contrast for ease of segmentation – very high current and significant post-scan image filtering can assist in producing good scan data.

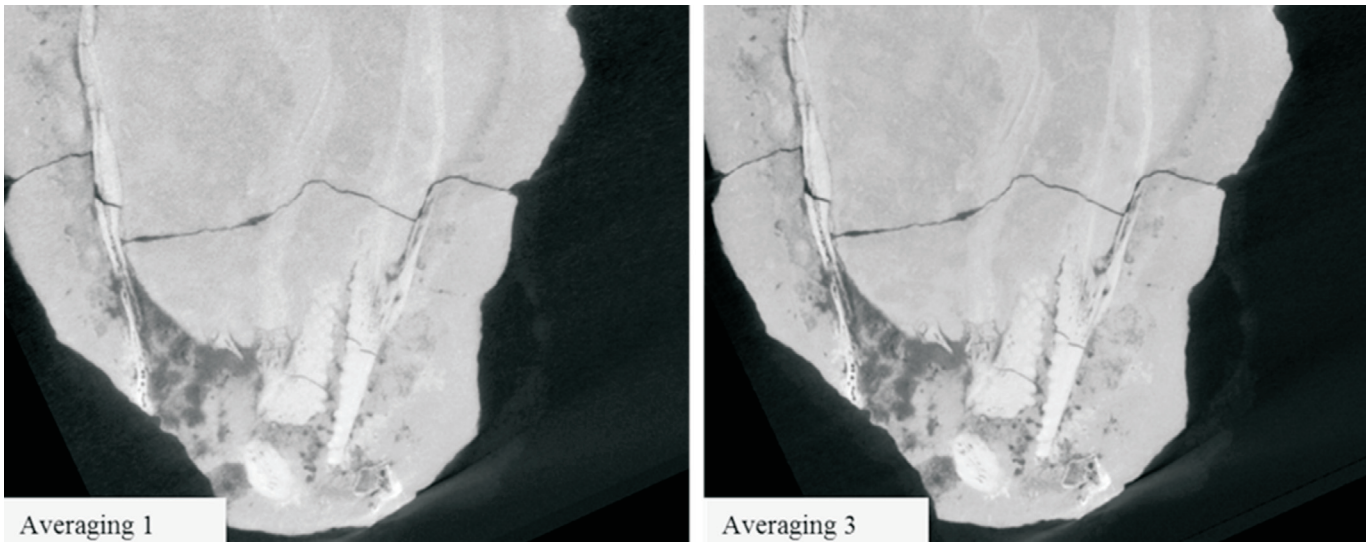

Figure 13. 2D slice images showing the quality change of varying image averaging.

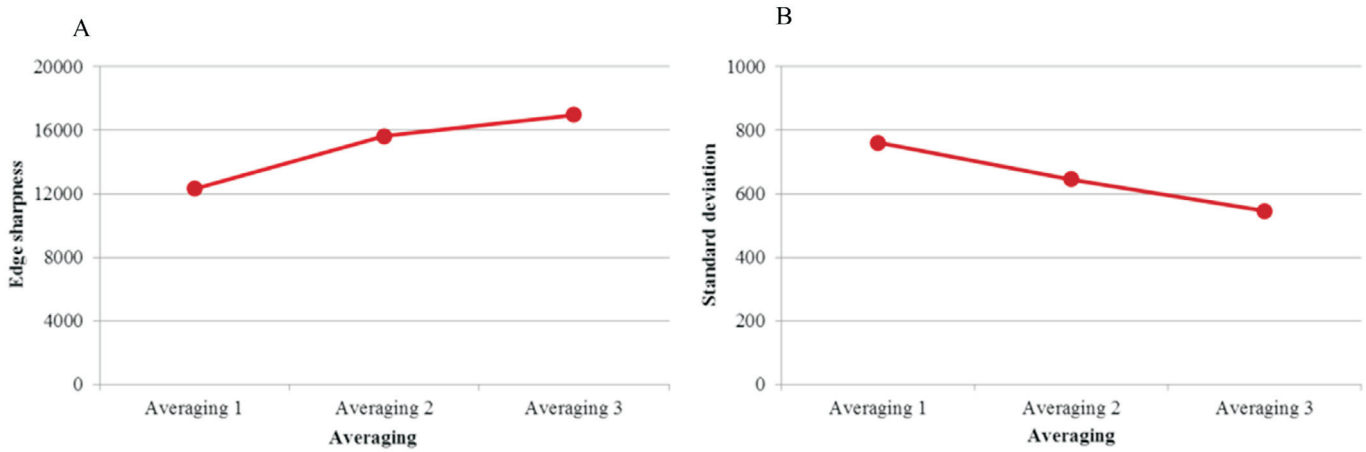

Figure 14. The effect of varying averaging on the image edge sharpness measured as the gradient of the slope between two materials, using the minimum and maximum values of the two (**A**) and background noise measured as the standard deviation of the mean grey values taken from the volume of the ROI (**B**).

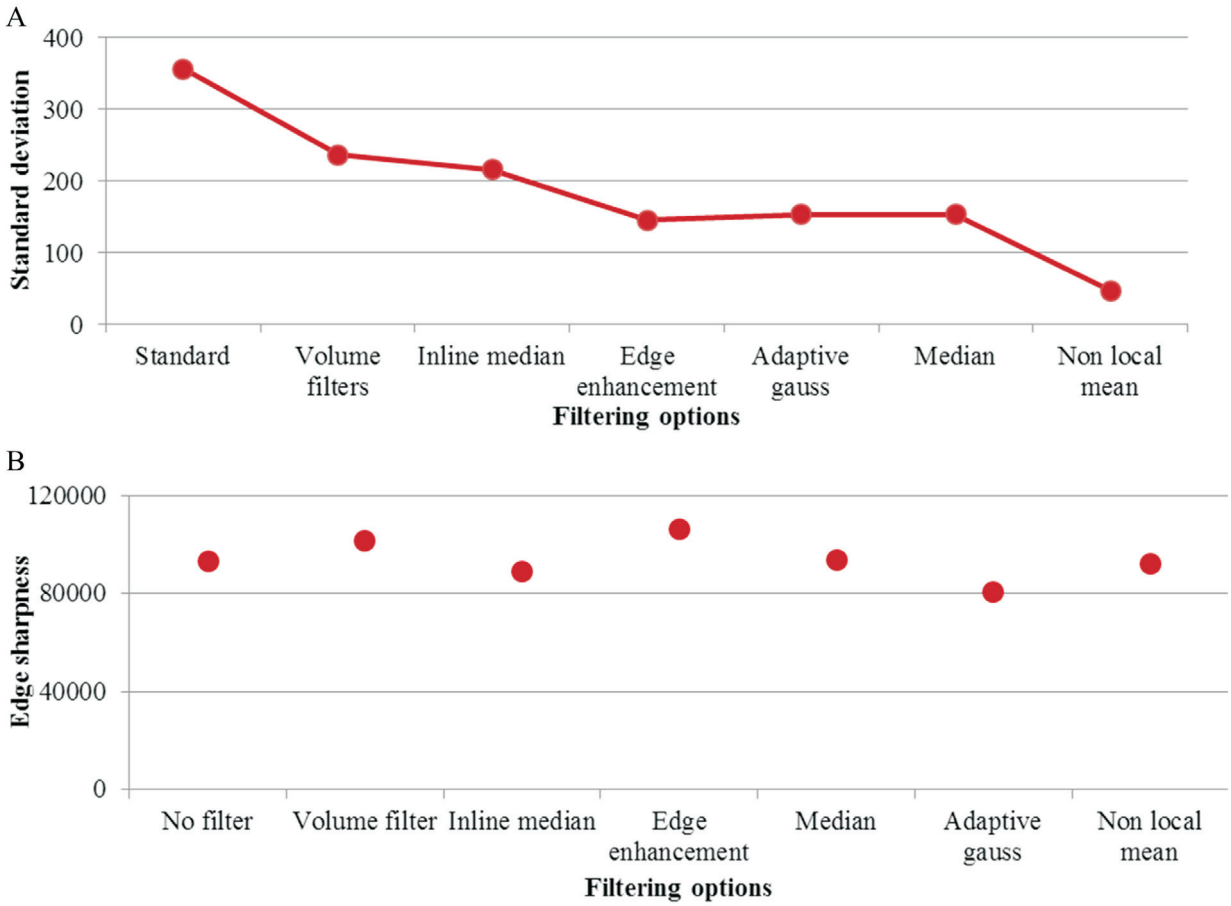

Figure 15. The effect of varying filtering options on the image edge sharpness measured as the gradient of the slope between two materials, using the minimum and maximum values of the two (**A**) and background noise measured as the standard deviation of the mean grey values taken from the volume of the ROI (**B**).

These results are specific for the tested sample, a 60 mm-thick, carbonate-rich, micritic mudstone nodule from the early Mid-Triassic (Anisian) Burgersdorp Formation of the Karoo Supergroup containing the complete skull and parts of the post-crania of a basal rhynchosaur. The best possible scan parameters are presented and we envisage this to be useful as a starting point for future paleontological studies using the microCT technique. The demonstrated optimized parameters are expected to be relevant to similar sample types and applicable to most rocks containing fossils. In particular the importance of X-ray intensity (current) was found to be much more than volt-

Table 1. Typical *vs* high quality scan.

Parameter	Typical	Final scan
Voltage	80 kV	120 kV
Current	100 μA	670 μA
Averaging	1	3
Beam filtering	–	0.2 mm Cu

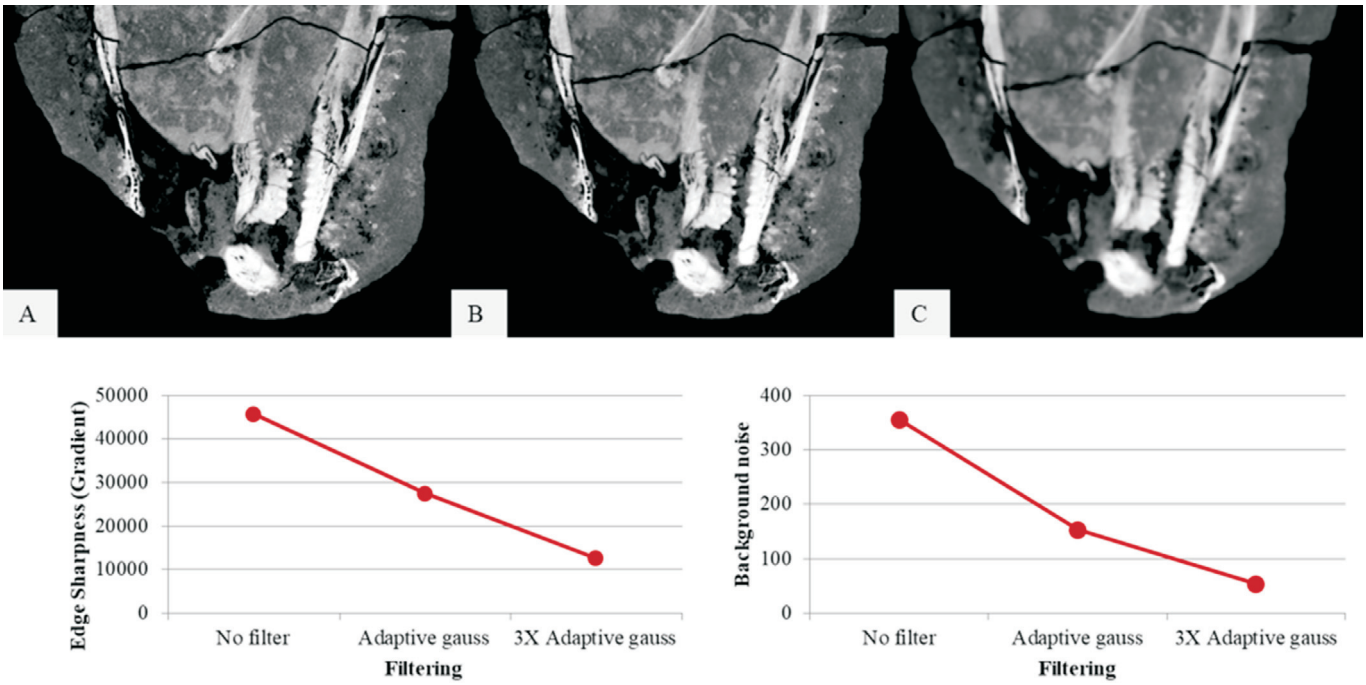

Figure 16. The effect of on increasing filtering on the image edge sharpness measured as the gradient of the slope between two materials, using the minimum and maximum values of the two (**A**) and background noise measured as the standard deviation of the mean grey values taken from the volume of the ROI (**B**). (A, Left) Unfiltered scan (B, middle) is the adaptive gauss and (**C**) is the 3X adaptive gauss filtered slice image.

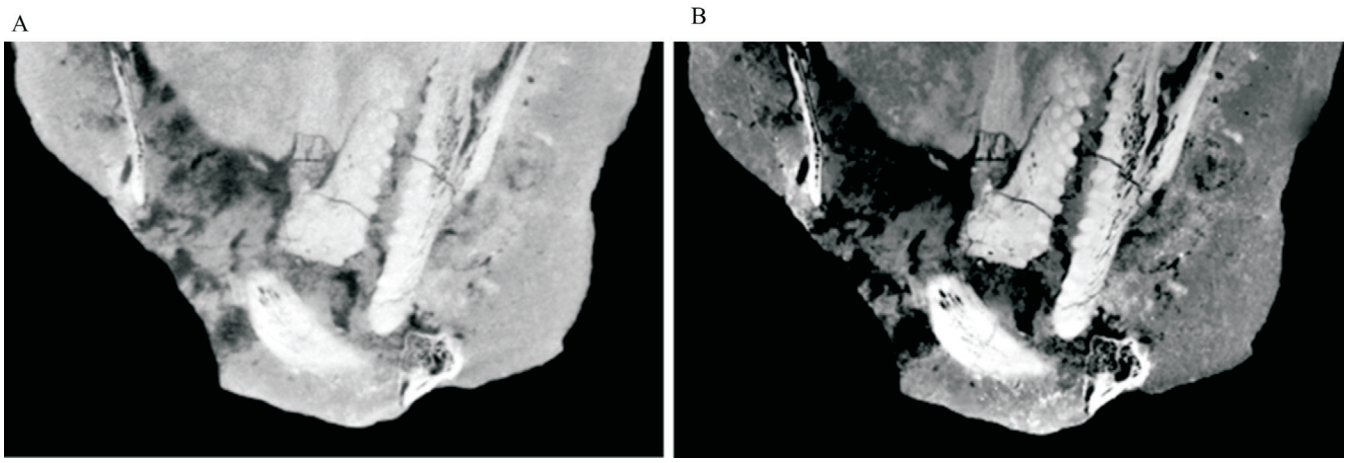

Figure 17. Comparison between a 2D slice image of a typical scan and final optimized scan.

age variation for high quality images of this sample type. Voltage reduction is usually recommended for discrimination of different materials (e.g. fossil bone – rock), but our results show that this is not always the case. The simulated fossil bone with surrounding rock supports this statement to some extent. The results are expected to be general for samples of varying composition and dimensions, but this case study did not particularly investigate how broadly this is applicable. We hope the approach presented (the quantitative assessment of image quality) may be useful to find optimal parameters for various fossil scans of different dimensions and compositions. The case study presented may be a good starting point for optimization in each case. Such optimized scans might also aid

Table 2. The effect of various parameters on the image quality obtained.

Parameters	Noise	Edge sharpness	Other comment	Overall image quality
Voltage increase	No effect	No effect	Increases X-ray penetration	No effect
Current increase	Improve	Improve	Increases the detector counts	Improves
Beam filtering increase	Worsen	Improve	Pre-compensate beam hardening	Improves
Frame averaging	Improve	Improve	Reduces noise	Improves
Beam hardening correction	Worsen	Improve	Removes cupping artefacts	Improves
Reconstruction filtering	Improve	No effect	Reduces noise but excessive filtering reduces edge sharpness	Improves
Post processing filtering	Improve	No effect	Reduces noise but excessive filtering reduces edge sharpness	Improves

Table 3. Parameters systematically investigated.

Voltage	Current	X-ray sensitivity
80 kV	100 μA	4
120 kV	40 μA	4
140 kV	70 μA	3
160 kV	60 μA	3
180 kV	50 μA	3
Current	**Voltage**	**Beam filter**
40 μA	120 kV	None
700 μA	120 kV	0.5 mm Cu
Beam filters	**Voltage**	**Current**
No beam filter	180 kV	70 μA
0.1 mm Cu	180 kV	70 μA
0.2 mm Cu	180 kV	220 μA
0.3 mm Cu	180 kV	140 μA
0.5 mm Cu	180 kV	110 μA
1 mm Cu	180 kV	90 μA
	Voltage	**Current**
Beam hardening correction	80 kV	300 μA
Filtering options	80 kV	300 μA
Averaging	180 kV	70 μA

the future development of automated laser fossil preparation systems using a combination of microCT and laser processing as demonstrated by Du Plessis *et al*. 2013.

§ORCID iDs

M. Tshibalanganda orcid.org/0000-0003-1933-5698
A. du Plessis: orcid.org/0000-0002-4370-8661
S.G. Le Roux: orcid.org/0000-0002-5617-8137
W.L. Taylor: orcid.org/0000-0002-9899-5864
R.M.H. Smith: orcid.org/0000-0001-6806-1983
C. Browning: orcid.org/0000-0003-1931-7502

REFERENCES

ABEL, R.L., LAURINI, C.R. & RICHTER, M. 2012. A palaeobiologist's guide to "virtual" micro-CT preparation. *Palaeontologia Electronica* **15**: 1–16.
DOI: palaeo-electronica.org/content/issue-2-2012-technical-articles/233-micro-ct-workflow

ARAÚJO, R., FERNANDEZ, V., RABBITT, R.D., EKDALE, E.G., ANTUNES, M.T., CASTANHINHA, R., FRÖBISCH, J. & MARTINS, R.M.S. 2018. Endothiodon cf. bathystoma (Synapsida: Dicynodontia) bony labyrinth anatomy, variation and body mass estimates. *PLOS ONE* **13**: e0189883.
DOI: 10.1371/journal.pone.0189883

BENOIT, J., MANGER, P.R., FERNANDEZ, V. & RUBIDGE, B.S. 2016. Cranial bosses of *Choerosaurus dejageri* (Therapsida, Therocephalia): earliest evidence of cranial display structures in eutheriodonts. *PLOS ONE* **11**: 1–23.
DOI: 10.1371/journal.pone.0161457

BENOIT, J., NORTON, L.A., MANGER, P.R. & RUBIDGE, B.S. 2017. Reappraisal of the envenoming capacity of *Euchambersia mirabilis* (Therapsida, Therocephalia) using μcT-scanning techniques. *PLOS ONE* **12**: 1–22.
DOI: 10.1371/journal.pone.0172047

CANTATORE, A & MÜLLER, P. 2011. Introduction to computed tomography. DTU Mechanical Engineering, Kgs. Lyngby, Copenhagen, Denmark. 72 pp.

CHAPELLE, K.E.J. & CHOINIERE, J.N. 2018. A revised cranial description of *Massospondylus carinatus* Owen (Dinosauria: Sauropodomorpha) based on computed tomographic scans and a review of cranial characters for basal Sauropodomorpha. *PeerJ* **6**: e4224.
DOI: 10.7717/peerj.4224

CNUDDE, V. & BOONE, M.N. 2013. High-resolution X-ray computed tomography in geosciences: a review of the current technology and applications. *Earth-Science Reviews* **123**: 1–17.
DOI: 10.1016/j.earscirev.2013.04.003

CUNNINGHAM, J.A., RAHMAN, I.A., LAUTENSCHLAGER, S., RAYFIELD, E.J. & DONOGHUE, P.C.J. 2014. A virtual world of paleontology. *Trends in Ecology and Evolution* **29**: 347–357.
DOI: 10.1016/j.tree.2014.04.004

DAWSON, M., FRANCIS, J. & CARPENTER, R. 2014. New views of plant fossils from Antarctica: a comparison of X-ray and neutron imaging techniques. *Journal of Paleontology* **88**: 702–707.

DU PLESSIS, A., STEYN, J., ROBERTS, D.E., BOTHA, L.R. & BERGER, L.R. 2013. A proof of concept demonstration of the automated laser removal of rock from a fossil using 3D X-ray tomography data. *Journal of Archaeological Science* **40**: 4607–4611.
DOI: 10.1016/j.jas.2013.07.024

DU PLESSIS, A., BROECKHOVEN, C., GUELPA, A. & GERHARD, S. 2017. Laboratory X-ray micro-computed tomography: a user guideline for biological samples. *Gigascience* **6**: 1–27.
DOI: 10.1093/gigascience/gix027

DU PLESSIS, A., LE ROUX, S.G. & GUELPA, A. 2016. The CT Scanner Facility at Stellenbosch University: an open access X-ray computed tomography laboratory. *Nuclear Instruments and Methods in Physics Research, Section B: Beam Interactions with Materials and Atoms* **384**: 42–49.
DOI: 10.1016/j.nimb.2016.08.005

FISHER, D., SHIRLEY, E., WHALEN, C. & CALAMARI, Z.2014. X-ray computed tomography of two mammoth calf mummies. *Journal of Paleontology* **88**: 666–675.

JASINOSKI, S.C., ABDALA, F. & FERNANDEZ, V. 2015. Ontogeny of the Early Triassic cynodont *Thrinaxodon liorhinus* (Therapsida): cranial morphology. *Anatomical Record* **298**: 1440–1464.
DOI: 10.1002/ar.23116

KETCHAM, R.A. & CARLSON, W.D. 2001. Acquisition, optimization and interpretation of X-ray computed tomographic imagery: applications to the geosciences. *Computers & Geosciences* **27**: 381–400.
DOI: 10.1016/S0098-3004(00)00116-3

KLAGES, M., 2013. A Micro-CT Analysis of the hominoid subnasal anatomy. Electronic Thesis and Dissertation Repository. 1543.
http://ir.lib.uwo.ca/etd/1543

LIU, Y., SCHOLTZ, G. & HOU, X. 2015. When a 520 million-year-old Chengjiang fossil meets a modern micro-CT – A case study. *Scientific Reports* **5**: 1–8.
DOI: 10.1038/srep12802

LUKENEDER, A., LUKENEDER, S. & GUSENBAUER, C. 2014. Computed tomography and laser scanning of fossil cephalopods (Triassic and Cretaceous). *Denisia* 32, *Zugleich Kataloge des Oberpsterreichischen Landesmuseums Neue Serie* **157**: 81–92.

LYSON, T.R., RUBIDGE, B.S., SCHEYER, T.M., DE QUEIROZ, K., SCHACHNER, E.R., SMITH, R.M.H., BOTHA-BRINK, J. & BEVER, G.S. 2016. Fossorial origin of the turtle shell. *Current Biology* **26**: 1887–1894.
DOI: 10.1016/j.cub.2016.05.020

RAHMAN, I. A., ADCOCK, K. & GARWOOD, R.J. 2012. Virtual fossils: a new resource for science communication in paleontology. *Evolution: Education and Outreach* **5**: 635–641.
DOI: 10.1007/s12052-012-0458-2

RAHMAN, I. A. & SMITH, S.Y. 2014. Virtual paleontology: computer-aided analysis of fossil form and function. *Journal of Paleontology* **88**: 633–635.
DOI: 10.1666/13-001I

REID, M., BORDY, E.M., TAYLOR, W.L., LE ROUX, S.G. & DU PLESSIS, A. 2018. A micro X-ray computer tomography dataset of fossil echinoderms in an ancient obrution bed: a robust method for taphonomic and palaeoecologic analyses. *GigaScience* **8**: 1–8.
http://dx.doi.org/10.5524/100539

SMILG, J.S. 2017. Finding fossils in Malapa breccia – medical CT scanning or micro-CT scanning? *South African Journal of Science* **113**: 1–6.
DOI: 10.17159/sajs.2017/20170057

SMITH, R.M.H. 2000. Sedimentology and taphonomy of Late Permian vertebrate fossil localities in southwestern Madgascar. *Palaeontologia africana* **36**: 25–41.

SMITH, R.M.H, RUBIDGE, B.S. & VAN DER WALT, M. 2011. Therapsid biodiversity patterns and paleoenvironments of the Karoo Basin, South Africa. **In**: Chinsamy-Turan, A. (ed.), *Forerunners of Mammals: Radiation, Histology, Biology*, 223–246. Bloomington, U.S.A., Indiana University Press.

SOBRAL, G., SOOKIAS, R.B., BHULLAR, B-A.S., SMITH, R., BUTLER, R.J. & MÜLLER, J. 2016. New information on the braincase and inner ear of *Euparkeria capensis* Broom: implications for diapsid and archosaur evolution. *Royal Society Open Science* **3**: 160072.
DOI: 10.1098/rsos.160072

SUTTON, M., RAHMAN, I. & GARWOOD, R. 2014. *Virtual, Techniques for Palaeontology*. Chichester, U.K., John Wiley & Sons.